CHEMISTRY OF MATERIALS

pubs.acs.org/cm

Article

Pressure Controls the Structure and Nonlinear Optical Properties of Piezochromic $CdTeMoO_6$

Dequan Jiang, Zimin Jiang, Huimin Song, Pei Wang, Hui Luo, Chen Li, Ke Liu, Ting Wen, Wenge Yang,* Yusheng Zhao, and Yonggang Wang*

Cite This: *Chem. Mater.* 2021, 33, 2929−2936

Read Online

HPSTAR 1181-2021

ACCESS | Metrics & More | Article Recommendations | Supporting Information

ABSTRACT: Materials with excellent nonlinear optical properties, especially the second-harmonic-generation (SHG) ability that can double the frequency of a laser ω to 2ω, are greatly important to modern optical technology. Recently, a temperature-induced SHG "on−off" phenomenon has been reported in dozens of metal−organic complexes, which have emerged as candidates in advanced optoelectronic applications. As a counterpart to temperature, pressure is also expected to trigger a SHG "on−off" phenomenon; nevertheless, such material is relatively limited. Herein, we report the observation of a pressure-induced SHG "on−off" phenomenon accompanied by a structural phase transition and piezochromism in $CdTeMoO_6$. Under ∼10 GPa compression, the material exhibits a sharp transition from the "SHG-on" state to the "SHG-off" state. Coupled with the SHG "on−off" phenomenon, a structural transition occurs from two-dimensional to three-dimensional due to the dramatic change in the coordination environments of Te^{4+} and Mo^{6+} from $[TeO_4]$ and $[MoO_4]$ tetrahedra to $[TeO_6]$ and $[MoO_6]$ octahedra, respectively. The suppression of stereoactive lone-pair electrons on Te^{4+} is considered to be responsible for the SHG-off state under high pressure. Piezochromism from colorless to black is also observed coupled with the SHG "on−off" phenomenon, which can be attributed to the hybridization between Mo 4d and O 2p orbitals. Moreover, we demonstrate that the "three-in-one" transition (structural transition, SHG on−off, and piezochromism) is irreversible at room temperature but reversible upon annealing at increased temperatures (230−350 °C) with SHG, lattice dimension and color returning to those of the initial state. All of these behaviors make $CdTeMoO_6$ a maneuverable pressure- and temperature-regulated SHG switching material with pragmatic multifunctionality.

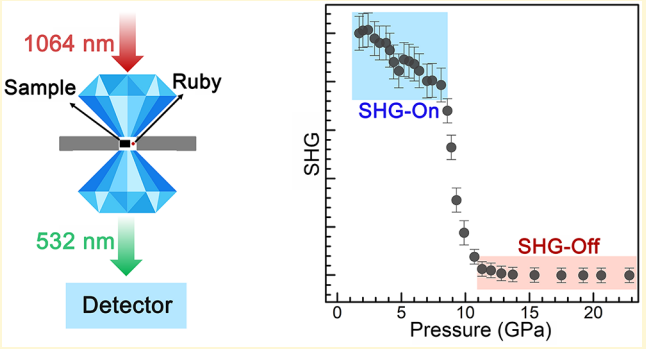

INTRODUCTION

As the lowest-order nonlinear optical (NLO) effect, second-harmonic generation (SHG) represents the ability of that material to convert two photons with a fundamental frequency ω to one photon with a doubled frequency 2ω. Due to the irreplaceable significance of frequency conversion of solid state lasers, SHG is frequently utilized to generate tunable coherent radiation in a wide region from ultraviolet (UV) to infrared (IR).[1,2] Therefore, the exploration of SHG materials plays a key role in the development of modern solid state laser technology, and several excellent SHG crystals have been discovered in the past two decades, such as BaB_2O_4 (BBO), LiB_3O_5 (LBO), $AgGaS_2$, and $ZnGeP_2$.[3−6] In particular, the $KBe_2BO_3F_2$ (KBBF) crystal can convert the 1064 nm Nd laser to a 177.3 nm deep-UV region via sixth-harmonic generation, which has been imminently employed in ultra-high-energy-resolution angle-resolved photoemission spectroscopy (ARPES).[7,8] Moreover, optical SHG is also a highly sensitive probe of the subtle magnetic orders in few-layer magnetic semiconductors, such as CrI_3,[9] and hidden phase transitions, interacting polarized sublattices, and interfaces in centrosymmetric or noncentrosymmetric magnetic oxides.[10]

Phase change materials accompanied by changes in physical properties are promising candidates for sensors, information storage, and switching devices.[11,12] The SHG behavior of a given material can also be tuned under external stimuli such as temperature and pressure. Numerous temperature-induced SHG switching materials have been reported in the past several decades. Characteristic examples include the order−disorder molecular rotor $[(Hdabco)(H_2O)Cl_3]$, the metal-free perovskite ferroelectrics MDABCO-NH_4I_3, and the displacive-type molecular ferroelectric 4-(cyanomethyl)anilinium perchlorate.[13−15] Most of them exhibit SHG "on−off" switching

Received: January 31, 2021
Revised: March 27, 2021
Published: April 7, 2021

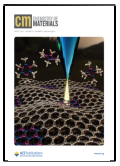

upon either cooling or heating along with structural phase transformations. Comparatively, pressure-induced SHG switching materials have rarely been reported, probably due to the lack of steepness for practical applications. In fact, pressure is a fundamental thermodynamic parameter that is as important as temperature and can act as a powerful tool to drive changes in structural or physical properties, including SHG.[16−18] Nevertheless, in previous studies, most of the compounds have exhibited unfavorable SHG change behaviors under compression, either an ambiguous or a gradual decrease over tens of gigapascals in SiO_2, $CaMnTi_2O_6$, Cr_2O_3, etc.[19−21] The exploration of more pressure-responsive SHG switching materials, especially those with sharp "on−off" phenomena fulfilling the requirements of a switch device, is urgently needed.

From the viewpoint of structure chemistry, SHG exists in only noncentrosymmetric crystal structures.[22] According to the "anionic group theory",[23,24] the overall SHG efficiency of a crystal is determined by the dividual polarity of asymmetrical units (e.g., triangles, lone-pair electrons, and distorted polyhedra) and their sum via periodic arrangement in the lattice. In this work, we report the results of high-pressure (HP) studies of a lone-pair electron-dominated SHG crystal $CdTeMoO_6$.[25] First, as pressure can weaken the stereoactivity of cations of lone electron pairs based on previous reports,[26−28] it is expected that the lone-pair electrons on the ($Te^{4+}O_4$) tetrahedra responsible for strong SHG efficiency can be suppressed under high pressure, and this gives an SHG "on−off" phenomenon. Second, $CdTeMoO_6$ is a quasi-two-dimensional (2D) material consisting of unsaturated coordination polyhedra (e.g., CdO_4, MoO_4, and TeO_4). The dramatic changes in the local coordination environments and a 2D to three-dimensional (3D) structural transformation are also expected in $CdTeMoO_6$, which may produce intriguing phenomena such as metallization. *In situ* HP structure analyses combined with Raman and infrared (IR) spectroscopy are performed and UV−vis−NIR absorption spectra are recorded to study the structure and property evolution of $CdTeMoO_6$. Finally, we also dig into the reversibility of the pressure-induced "three-in-one" transition in $CdTeMoO_6$. The discovery of a pressure- and temperature-regulated SHG switching material, the multifunctionality, and the maneuverable control method together shed light on the future exploration of SHG switching materials.

EXPERIMENTAL SECTION

Sample Preparation. The reaction reagents were TeO_2 (Aladdin, 99.99%), MoO_3 (Macklin, 99.99%), and CdO (Aladdin, 99.99%).

A polycrystalline sample of $CdTeMoO_6$ was synthesized using the traditional solid state method. Stoichiometric ratios of TeO_2 (0.320 g, 2 mmol), MoO_3 (0.288 g, 2 mmol), and CdO (0.257 g, 2 mmol) were thoroughly mixed and placed in a corundum crucible. The crucible was then heated to 700 °C and held for 72 h with several intermediate grindings. Finally, phase-pure $CdTeMoO_6$ powder was obtained for further measurements.

Single crystals of $CdTeMoO_6$ were obtained by the spontaneous crystallization approach. A Pt crucible with pure $CdTeMoO_6$ powder was placed in the center of a muffle furnace. The temperature was increased to 900 °C and held for 10 h to guarantee the melt was homogeneous. Then the crucible was cooled slowly to 600 °C and rapidly to room temperature. Transparent $CdTeMoO_6$ crystals were obtained.

***In Situ* HP Experiments.** A symmetric diamond anvil cell (DAC) with type II diamonds polished to a diameter of 500 μm was employed to generate high pressure. Steel gaskets were preindented to ~40 μm thick, and then 250 μm holes were drilled as the sample chambers. The denser sample and ruby balls were placed in the sample chamber. To keep the experimental conditions consistent, inert silicone oil was employed as the pressure medium for all of the high-pressure measurements. The pressure was calibrated on the basis of the fluorescence peak of the ruby balls.[29]

In situ HP XRD measurements were recorded at the BL15U1 beamline station of Shanghai Synchrotron Radiation Facility (SSRF) at room temperature. An MAR165 CCD detector was used to record the *in situ* HP XRD patterns, and CeO_2 was chosen as the calibration standard. DIOPTAS software was used to perform data reduction.[30] Cell parameters under different pressures were refined by the LeBail method using FULLPROF.[31]

In situ HP Raman spectra were recorded on a Renishaw Raman microscope using a 532 nm laser. The system was calibrated by the Raman signal of Si, and spectra were collected in the range of 100−1100 cm^{-1}.

In situ HP IR spectra were recorded on a Bruker VERTEX 70v IR spectrometer with a HYPERION 2000 microscope. A Globar was used as a conventional source. The spectra were recorded in absorption mode in the range of 600−1500 cm^{-1} with a resolution of 2 cm^{-1}. The spectrum of a DAC full of KBr under ambient conditions in the same aperture region was used as the background.

In situ HP UV−vis−NIR absorption spectra were recorded using a Xeon light source between 300 and 1100 nm. The absorption spectra and optical images were obtained in a homemade spectroscopy system in the microregion (Gora-UVN-FL, Ideaoptics, Shanghai, China). The bandgap is determined by extrapolating the linear portion of the $\alpha^{1/2}$ versus $h\nu$ curve, where α is the absorption coefficient, h is Planck's constant, and ν is the frequency of the photon.[32]

The *in situ* HP SHG experiment was performed in a homemade optical system. A fiber laser (NPI LASER Co., Ltd., 1064 nm, 20 MHz, 15 ps) was used as the exciting light source, and the laser spot was focused to 40 μm. A photomultiplier tube (Thorlabs, Inc., PMT1000) was employed to collect the SHG signal. The HP SHG measurement is based on the ambient powder SHG measurement extended by Kurtz and Perry.[33]

Density Functional Theory (DFT) Calculations. The calculations were performed using the VASP package. Two $CdTeMoO_6$ structures, one with an orthorhombic symmetry (ICSD 93794) and the other in space group $P2_1$, were adopted as the initial structure models for the LP and HP phases, respectively. The cell parameters of the HP structure were from the LeBail fitting of the powder XRD spectra at 13.2 GPa and followed by structure optimization. The electron−electron interaction is treated using the LDA and PAW−PBE pseudopotential, with an energy cutoff of 600 eV. The valence electronics of Cd, Te, Mo, and O are $4d^{10}\ 5s^2$, $5s^2\ 5p^4$, $4d^5\ 5s^1$, and $2s^2\ 2p^4$, respectively.

RESULTS AND DISCUSSION

Material Syntheses and Ambient Crystal Structure. $CdTeMoO_6$ was first reported in the 1970s,[34,35] and the crystal structure was determined in 2001.[36] In 2013, Zhao et al. confirmed its crystal structure by the single-crystal X-ray diffraction (XRD) method and characterized it as a promising SHG material.[25] In this work, a highly pure polycrystalline sample of $CdTeMoO_6$ was synthesized using the traditional solid state method (Figure S1). Single crystals of $CdTeMoO_6$ were obtained using the spontaneous crystallization method by melting the stoichiometric polycrystalline sample. Under ambient conditions, $CdTeMoO_6$ crystallizes in tetragonal space group $P\bar{4}2_1m$, with the following cell parameters: a = 5.2860(7) Å, and c = 9.0660(18) Å. The quasi-2D structure of $CdTeMoO_6$ consists of [$Te^{4+}O_4$] with stereoactive lone-pair electrons (mostly contributed to the overall SHG efficiency), distorted [MoO_4] tetrahedra, and regular [CdO_4] tetrahedra.

https://doi.org/10.1021/acs.chemmater.1c00362
Chem. Mater. 2021, 33, 2929−2936

Pressure-Induced Structural Phase Transformation. The *in situ* HP XRD experiment was conducted to understand the structure evolution of $CdTeMoO_6$ under compression. Figure 1a shows the powder XRD patterns of $CdTeMoO_6$ as a

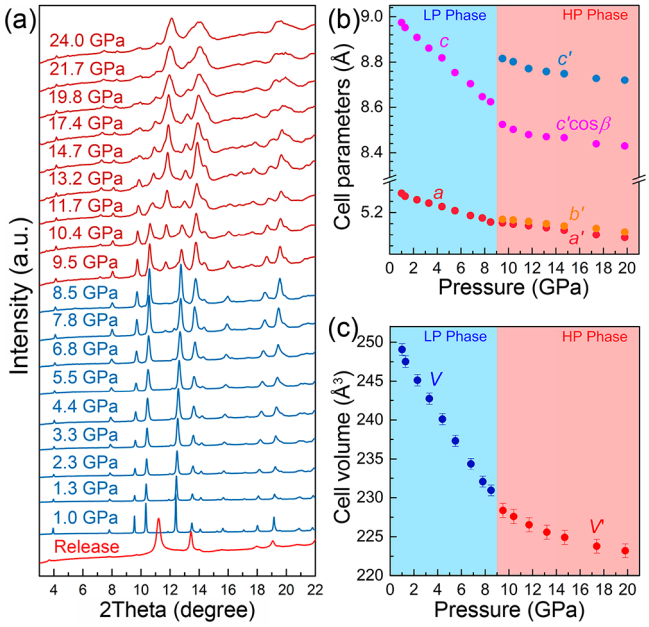

Figure 1. (a) *In situ* HP XRD patterns of $CdTeMoO_6$ at selected pressures, (b) cell parameters, and (c) cell volumes as a function of applied pressure for the LP and HP phases.

function of pressure. From ambient pressure to ~6.6 GPa, no phase transition occurs and all of the diffraction peaks can be indexed well in space group $P\bar{4}2_1m$. Although the phase can also be indexed well in space group $P\bar{4}2_1m$, in the 7.8 and 8.5 GPa patterns, the new reflection just below 12° is weakly visible, which suggests that a phase transition will take place. Upon >9.5 GPa compression, some of the old peaks weaken to disappear gradually and new peaks emerge, implying the occurrence of a phase transition. The phase transition reaches completion around 13.2 GPa, and the HP phase can persist to 24.0 GPa, the highest pressure in the XRD experiments. Notably, the pressure-induced phase transition of $CdTeMoO_6$ is irreversible as the XRD pattern does not return to the original form after the pressure is released.

The XRD patterns of the HP phase of $CdTeMoO_6$ can be indexed in monoclinic space group $P2_1$, a subgroup of initial space group $P\bar{4}2_1m$ under ambient conditions. At 13.2 GPa, the refined cell parameters are as follows: a = 5.1454(9) Å, b = 5.1641(7) Å, c = 8.7585(6) Å, β = 93.0(1)°. Panels b and c of Figure 1 show the cell parameters of $CdTeMoO_6$ as a function of applied pressure. For the low-pressure (LP) phase, the c axis shrinks faster than the a axis, probably due to the higher compressibility caused by the interlayer empty space. An abrupt decrease in c'*cos β compared with c indicates a lattice collapse along the c axis during the phase transition. For the HP phase, all of the cell parameters decrease at a similar rate with an increase in pressure, and the HP phase is obviously harder than the LP phase.

Pressure-Induced SHG "On−Off" Transition. According to a previous study,[25] $CdTeMoO_6$ exhibits a strong SHG response at ambient pressure (approximately twice that of $KTiOPO_4$ at 1064 nm), which makes it a potential candidate for near-IR and mid-IR laser conversion. The *in situ* HP SHG measurement of $CdTeMoO_6$ was conducted at room temperature using a homemade optical system (Figure 2a; see the Experimental Section for details). SHG-inert silicone oil was employed as the pressure transmission medium to avoid any interference.

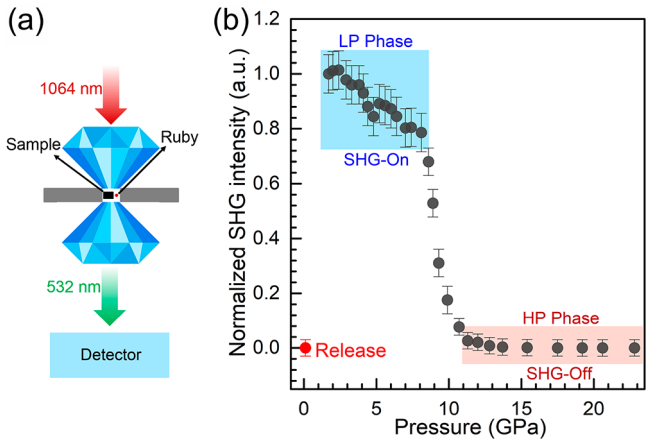

Figure 2. (a) Sketch map of *in situ* HP SHG measurement. (b) Pressure dependence of the SHG intensity of $CdTeMoO_6$ during compression.

Figure 2b displays the SHG intensity of $CdTeMoO_6$ as a function of pressure. At pressures of <8 GPa, the LP phase of $CdTeMoO_6$ exhibits strong SHG responses and the SHG intensity decreases slightly due to the pressure effect (such as strain, amorphous, and particle size change). As the pressure increases beyond 8 GPa, the SHG intensity decreases rapidly, which is quite consistent with the pressure-induced phase transition. $CdTeMoO_6$ loses all of the SHG intensity above 11.3 GPa, indicating that the HP phase of $CdTeMoO_6$ is SHG-inactive. Notably, no SHG signal is detected from the released sample, which indicates that the SHG "on−off" phenomenon of $CdTeMoO_6$ is also irreversible in parallel with the pressure-induced phase transition.

Compared with compounds in previous SHG-related studies under high pressure, $CdTeMoO_6$ represents the rare example of a SHG "on−off" material potential for practical applications. In the past, HP SHG measurements were mostly employed as a tool for lattice or magnetic structure changes, for example, the pressure-induced B4 to B1 phase transition of ZnO[37] and the pressure-induced magnetic transition of Cr_2O_3.[21] In these materials, most of the pressure-induced SHG changes are either ambiguous or gradual. To the best of our knowledge, only ZnO contains the similarly sharp SHG "on−off" phenomenon like $CdTeMoO_6$. However, compared with ZnO, the advantage of $CdTeMoO_6$ is the stronger SHG effect in the SHG "on" state. In addition, for a functional switch material, the transition should be sharp and the "on" and "off" states should be relatively stable. According to the SHG measurements in this work, the irreversible "SHG-on" to "SHG-off" change in $CdTeMoO_6$ is steep and clear enough to make it a potential pressure-responsive SHG "on−off" material.

Pressure-Induced 2D to 3D Structural Transition. During the pressure-induced phase transition around 9 GPa, a lattice collapse occurs along the c axis as evidenced from the cell parameter analyses. The crystal structure of the HP phase

https://doi.org/10.1021/acs.chemmater.1c00362
Chem. Mater. 2021, 33, 2929−2936

of $CdTeMoO_6$ is determined by combining the XRD refinements (Figure S2 and Table S1), structure optimization by theoretical calculations, and local structure analyses (will be discussed in the section on Raman and IR spectra). The DFT relaxation of the HP structure starts from an initial structure model with experimental cell parameters at 13.2 GPa and atomic coordinates at ambient pressure. The optimization under high pressure is done with preindexed space group $P2_1$ without any restraints. Figure 3 shows the crystal structures of

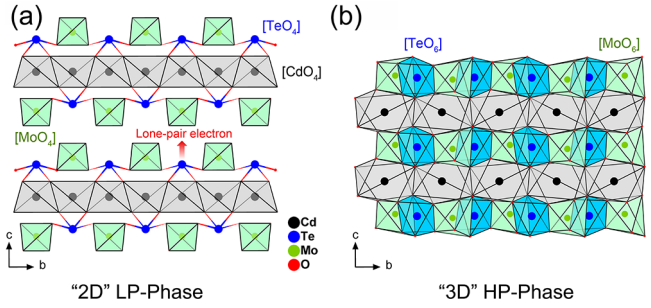

Figure 3. Crystal structures of (a) the LP phase and (b) the HP phase of $CdTeMoO_6$.

the LP and HP phases of $CdTeMoO_6$. An obvious 2D to 3D transformation happens during the pressure-induced phase transition, which can be considered the result of the evolution of the coordination environment of cations Cd^{2+}, Te^{4+}, and Mo^{6+}. Under compression, the coordination number of Te^{4+} and Mo^{6+} increases from 4 for $[TeO_4]$ and $[MoO_4]$ tetrahedra to 6 for $[TeO_6]$ and $[MoO_6]$ octahedra, respectively, which primarily contributes to the 2D to 3D structural transition. In the 3D HP phase of $CdTeMoO_6$, the basic structure units are $[TeO_6]$, $[MoO_6]$, and distorted $[CdO_8]$. The degeneration of the lone-pair electrons on $[TeO_4]$ tetrahedra and the d orbital rearrangement of Mo^{6+} will inevitably affect the physical properties of $CdTeMoO_6$. It is worth mentioning that the calculated BVS values for Te and Mo based on the optimized HP structure at 13.2 GPa are +4.8 and +3.6, respectively, which indicates the possibility of charge transfer between the two metal centers, but further experimental evidence is needed.

Piezochromism and Pressure-Induced Bandgap Narrowing. Pressure is an effective tool for regulating the optical and electrical properties of a given material and triggers unexpected phenomena at high pressures, such as metallization and piezochromism.[38−40] At ambient pressure, $CdTeMoO_6$ is an indirect-bandgap and colorless semiconductor with an E_g value of 3.59 eV.[25,41] Under compression, $CdTeMoO_6$ exhibits an obvious colorless-to-black change as shown in Figure 4a. Notably, the color change of $CdTeMoO_6$ seems stepwise: it remains almost transparent and colorless before the pressure-induced phase transition around 9 GPa; after that, it quickly becomes yellow and finally opaque black above 20 GPa. *In situ* HP UV−vis−NIR absorption measurements are performed to gain additional information about the color change and the variation of the bandgap, as shown in panels b and c of Figure 4. We can conclude that the piezochromism of $CdTeMoO_6$ is mainly due to the pressure-induced bandgap narrowing. Below 7.6 GPa, the absorption edge of $CdTeMoO_6$ slowly shifts to longer wavelengths, and the bandgap decreases by ∼0.27 eV compared with the ambient value. Then the bandgap decreases rapidly by ∼1 eV in the range of 7.6−11.5 GPa. The dramatic color change and bandgap narrowing are coupled with both

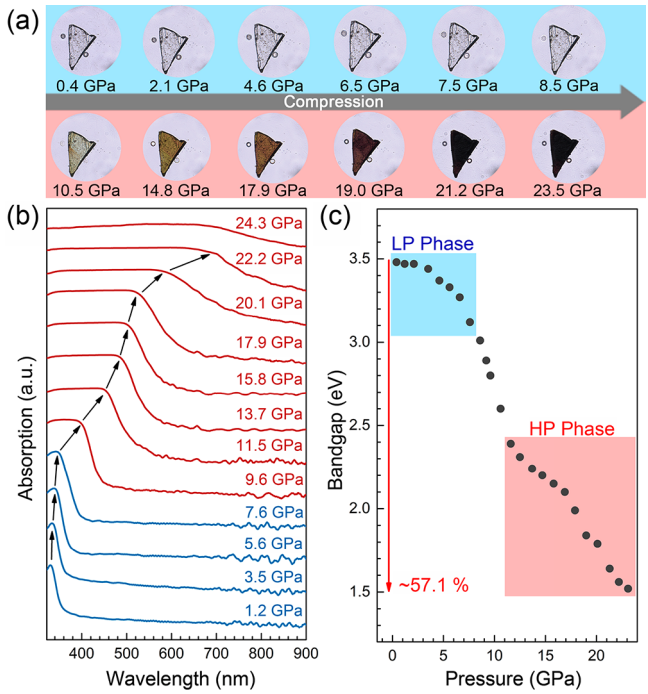

Figure 4. (a) Optical photos of $CdTeMoO_6$ during compression. (b) *In situ* UV−vis−NIR absorption spectra of a single crystal of $CdTeMoO_6$ under compression. (c) Pressure dependence of the bandgaps of $CdTeMoO_6$.

the structural phase transition and the SHG "on−off" phenomenon. The bandgap of $CdTeMoO_6$ decreases by ∼57.1% during the whole compression up to 24.3 GPa. Moreover, the released sample does not return to the ambient condition (Figure S3), which implies that the piezochromism in $CdTeMoO_6$ is also irreversible.

Preliminary DFT calculations are carried out to reveal the mechanism of piezochromism and bandgap narrowing in $CdTeMoO_6$, neglecting the quantitative underestimation of the band introduced by the discontinuity of the exchange-correlation energy (Figure S4).[42] The valence band maximum (VBM) and conduction band minimum (CBM) of $CdTeMoO_6$ are mainly comprised of the O 2p and Mo 4d orbits, respectively. With an increase in pressure, the CBM orbitals (O 2p and Mo 4d) shift to the Fermi level, corresponding to the experimental results. Therefore, one can conclude that the change in the coordination environment of Mo^{6+} (from $[MoO_4]$ to $[MoO_6]$ groups) plays a key role in the piezochromism and giant bandgap narrowing in $CdTeMoO_6$. One can also predict that $CdTeMoO_6$ may suffer a metallization when the pressure increases slightly. It is worth mentioning that the piezochromism effect may also cause SHG to decrease due to self-absorption at 532 nm. In the case of $CdTeMoO_6$, the pressure-induced SHG-off behavior is mainly due to the local structure evolution, because the SHG-off behavior happens far ahead before it becomes opaque at 532 nm (∼18 GPa).

Local Structure Evolution under Compression. As discussed above, the pressure-induced SHG "on−off", piezochromism, and 2D to 3D structural transitions are all strongly related to the coordination environments of the cations. *In situ* HP Raman and IR spectra are collected to probe the local structure evolution in $CdTeMoO_6$ under compression. Figure 5 presents the pressure dependence of

https://doi.org/10.1021/acs.chemmater.1c00362
Chem. Mater. 2021, 33, 2929−2936

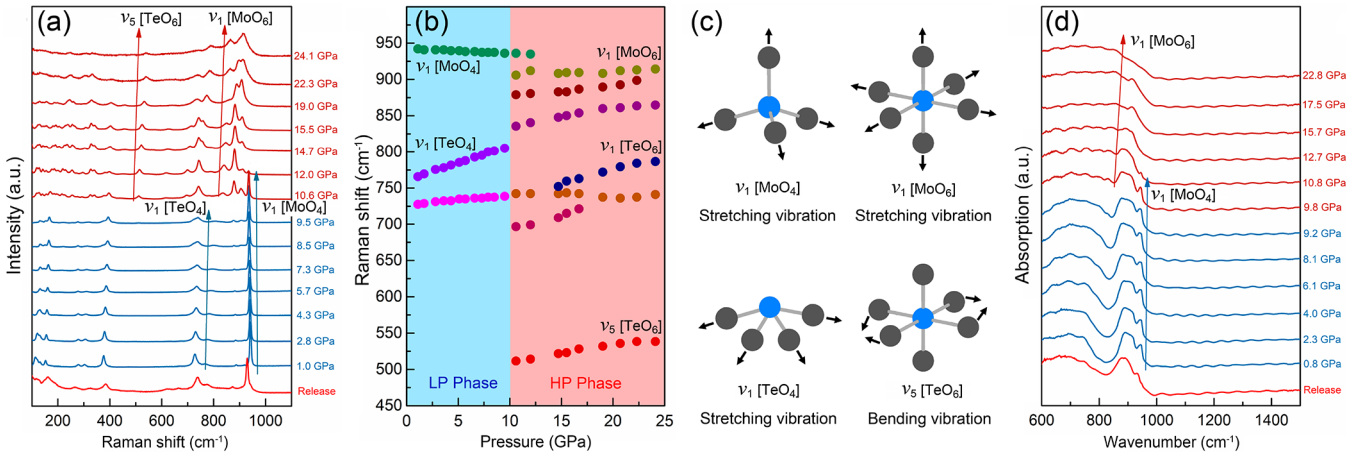

Figure 5. (a) *In situ* HP Raman spectra of $CdTeMoO_6$ at selected pressures. (b) Pressure dependence of the Raman peak positions in the wavenumber range of 450−1000 cm^{-1}. (c) Representative Raman vibrational modes of $[MO_4]$ tetrahedra and $[MO_6]$ octahedra (M = Mo or Te). (d) *In situ* HP IR spectra of $CdTeMoO_6$ at selected pressures.

Raman and IR spectra in wavenumber ranges of 100−1100 and 600−1500 cm^{-1}, respectively. The Raman and IR peaks around 930 cm^{-1} are the characteristic symmetric stretching vibration mode (ν_1) of $[MoO_4]$ tetrahedra, and the Raman peaks around 765 cm^{-1} are from the stretching vibration mode (ν_1) of $[TeO_4]$.

Before the pressure-induced transition, both Raman and IR peaks maintain the original profile with gradual peak shifts. As the pressure reaches 9.5 GPa, two small peaks at 877 and 906 cm^{-1} are visible in the Raman spectrum, which implies the beginning of the phase transition. When the pressure further increases above 10 GPa, dramatic changes take place in both the Raman and IR spectra, indicating remarkable changes in the local structures in $CdTeMoO_6$. First, three new peaks at 906, 877, and 836 cm^{-1} can be attributed to the stretching vibrations (ν_1) of $[MoO_6]$ octahedra. Second, the Raman softening implies an increase in Mo−O bond length from $[MoO_4]$ to $[MoO_6]$.[43,44] A $[TeO_4]$ to $[TeO_6]$ transformation is also observed around 10 GPa, as the stretching vibrations (ν_1) of $[TeO_4]$ at 730 and 765 cm^{-1} vanishes and two new peaks at 697 and 512 cm^{-1} emerge, corresponding to the stretching vibration (ν_1) and bending vibration (ν_5) of $[TeO_6]$ groups, respectively.[45,46] Detailed assignments of observed Raman modes are listed in Table S2. All of this evidence confirms the increase in the coordination numbers of Te^{4+} and Mo^{6+} from 4 to 6 during the pressure-induced structure transformation. The confirmation of the suppression of the stereoactive lone pairs on $[TeO_4]$ and the 4d orbital rearrangement of Mo^{6+} also match well with the SHG "on−off" and piezochromism phenomena. Although the Raman and IR spectra of the released sample are similar to those of the ambient phase (Figure 5a,d), the peak positions are still different and have obvious shifts. It is normal that there is a similar vibration energy but from distinct coordination groups.

Pressure- and Temperature-Regulated Binary State Switch. The irreversibility of the pressure-induced "three-in-one" transition is confirmed by the results of *in situ* XRD, absorption, and SHG measurements. Both Raman and IR spectra indicate that the local structures of the released HP phase are somehow similar to that of the LP phase. To further verify the structural relationship between the LP and HP phases, annealing experiments on the pressure-released $CdTeMoO_6$ are conducted and the products are monitored by Raman and SHG responses.

Figure 6a shows the Raman spectra of pressure-released $CdTeMoO_6$ upon annealing at different temperatures compared with the initial LP phase. Then, a new peak around 940 cm^{-1} emerges corresponding to the symmetric stretching vibration mode (ν_1) of $[MoO_4]$, indicating the coexistence of $[MoO_4]$ and $[MoO_6]$ and the partial phase recovery to the LP phase. After annealing at 350 °C for 20 h, the characteristic ν_1

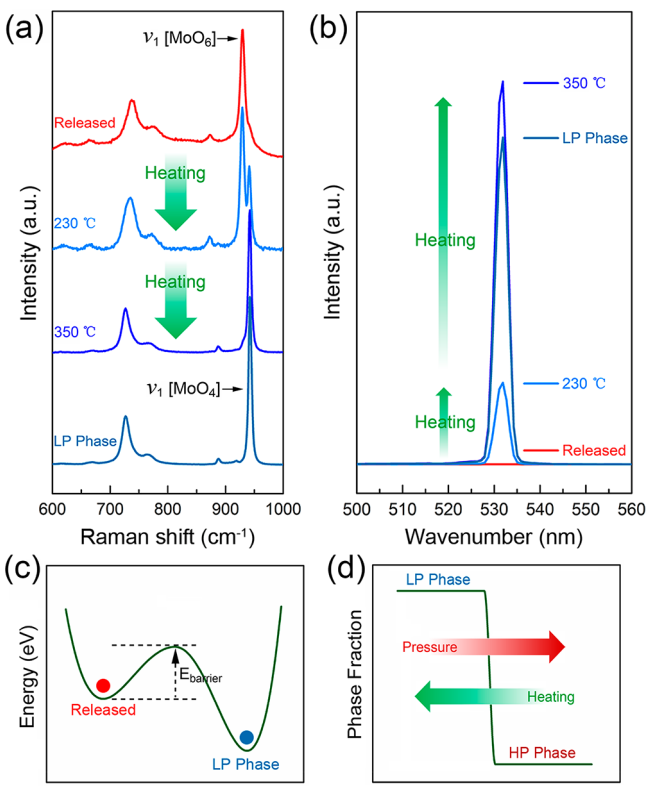

Figure 6. (a) Raman spectra and (b) SHG signals of pressure-released $CdTeMoO_6$ upon annealing at different temperatures compared with the initial LP phase. (c and d) Schematic diagrams of the total energy and phase fraction, respectively, between the HP phase and LP phase of $CdTeMoO_6$ upon heating and compression.

https://doi.org/10.1021/acs.chemmater.1c00362
Chem. Mater. 2021, 33, 2929−2936

vibration peak of [MoO_6] disappears completely and the overall Raman profile seems to be almost the same with the LP phase. SHG signals show the same changing process (Figure 6b), which confirms the temperature-driven HP phase to LP phase transformation at a relatively low temperature. A similar phenomenon occurs in ZnO,[37] which undergoes an irreversible phase transition, and heating aids in the recovery to the ambient wurtzite phase.

The dual regulation of the binary states in $CdTeMoO_6$ separately by pressure and temperature is illustrated in panels c and d of Figure 6. First, the pressure-induced structural phase transition, the SHG "on−off" transition, and piezochromism are irreversible at room temperature. The released HP phase is metastable compared with the LP phase, and there is an energy barrier to overcome to return to the LP phase. Second, both pressure and temperature can regulate the one-way "on−off" transition between the two states of $CdTeMoO_6$, and it is also possible to realize a cycling process. Finally, it is worth emphasizing that $CdTeMoO_6$ represents the SHG "on−off" transition and piezochromism coupled with the controllable structure regulation, both of which are significant functionalities that have potential to be used as switches or sensors.

CONCLUSION

In summary, we report a pressure- and temperature-regulated SHG switching in $CdTeMoO_6$. The sharp SHG "on−off" phenomenon is accompanied by a 2D to 3D structural phase transformation and a colorless to black piezochromism around 10 GPa. Structural analyses based on the combination of XRD data and Raman and IR spectra provide a clear understanding of the structure−property relationship. That is, the suppression of stereoactive lone-pair electrons on the Te^{4+} cations during the [TeO_4] to [TeO_6] transformation under compression triggers the "SHG-on" to "SHG-off" behavior. On the contrary, piezochromism and the large bandgap reduction are attributed to the increased degree of hybridization between the Mo 4d and O 2p orbitals along with the [MoO_4] to [MoO_6] transformation. Moreover, the pressure-induced "three-in-one" transition (structure transition, SHG on−off transition, and piezochromism) is irreversible at room temperature, but the metastable HP phase can return to the ambient phase after annealing at higher temperatures (230−350 °C, far below the synthesis temperature). The SHG response and the color return to ambient conditions, as well. Our demonstration of the development of the pressure-induced SHG "on−off" transition together with dramatic structure transition and piezochromism opens the door for future exploration of pressure-responsive bistable and multifunctional materials.

ASSOCIATED CONTENT

Supporting Information

The Supporting Information is available free of charge at https://pubs.acs.org/doi/10.1021/acs.chemmater.1c00362.

XRD refinement, LeBail fitting results, absorption spectra, calculated PDOS, structure information, and Raman assignments (PDF)

AUTHOR INFORMATION

Corresponding Authors

Wenge Yang − *Center for High Pressure Science and Technology Advanced Research (HPSTAR), Beijing 100094, China*; Email: yangwg@hpstar.ac.cn

Yonggang Wang − *Center for High Pressure Science and Technology Advanced Research (HPSTAR), Beijing 100094, China*; orcid.org/0000-0003-4816-9182; Email: yonggang.wang@hpstar.ac.cn

Authors

Dequan Jiang − *Center for High Pressure Science and Technology Advanced Research (HPSTAR), Beijing 100094, China*; orcid.org/0000-0003-0998-5507

Zimin Jiang − *Center for High Pressure Science and Technology Advanced Research (HPSTAR), Beijing 100094, China*

Huimin Song − *Beijing Center for Crystal Research and Development, Key Laboratory of Functional Crystals and Laser Technology, Technical Institute of Physics and Chemistry, Chinese Academy of Sciences, Beijing 100190, P. R. China*; orcid.org/0000-0002-2329-0704

Pei Wang − *Academy for Advanced Interdisciplinary Studies, Department of Physics, Southern University of Science and Technology, Shenzhen 518055, P. R. China*

Hui Luo − *Center for High Pressure Science and Technology Advanced Research (HPSTAR), Beijing 100094, China*

Chen Li − *Center for High Pressure Science and Technology Advanced Research (HPSTAR), Beijing 100094, China*

Ke Liu − *Center for High Pressure Science and Technology Advanced Research (HPSTAR), Beijing 100094, China*

Ting Wen − *Center for High Pressure Science and Technology Advanced Research (HPSTAR), Beijing 100094, China*; orcid.org/0000-0001-6572-0920

Yusheng Zhao − *Academy for Advanced Interdisciplinary Studies, Department of Physics, Shenzhen Key Laboratory of Solid State Batteries, Guangdong Provincial Key Laboratory of Energy Materials for Electric Power, Southern University of Science and Technology, Shenzhen 518055, P. R. China*

Complete contact information is available at: https://pubs.acs.org/10.1021/acs.chemmater.1c00362

Notes

The authors declare no competing financial interest.

ACKNOWLEDGMENTS

This work was supported by the National Natural Science Foundation of China (Grant 52073003), the Major Program of the National Natural Science Foundation of China (22090041), the National Key R&D Program of China (2018YFA0305900), and the Guangdong Provincial Key Laboratory of Energy Materials for Electric Power (2018B030322001). High-pressure XRD data were collected at beamline station BL15U1 of Shanghai Synchrotron Radiation Facility (SSRF), Shanghai, China.

REFERENCES

(1) Chen, C. T.; Bai, L.; Wang, Z. Z.; Li, R. K. Development of new NLO crystals for UV and IR applications. *J. Cryst. Growth* **2006**, *292*, 169−178.

(2) Becker, P. Borate materials in nonlinear optics. *Adv. Mater.* **1998**, *10*, 979−992.

(3) Chen, C.; Wu, B.; Jiang, A.; You, G. A new-type ultraviolet SHG crystal—β-BaB_2O_4. *Sci. Sin. B* **1985**, *28*, 235−243.

(4) Chen, C.; Wu, B.; Jiang, A.; Wu, B.; You, G.; Li, R.; Lin, S. New nonlinear-optical crystal: LiB_3O_5. *J. Opt. Soc. Am. B* **1989**, *6*, 616−621.

(5) Boyd, G. D.; Kasper, H.; McFee, J. H. Linear and nonlinear optical properties of $AgGaS_2$, $CuGaS_2$, and $CuInS_2$, and Theory of the

wedge technique for the measurement of nonlinear coefficients. *IEEE J. Quantum Electron.* **1971**, *7*, 563−573.
(6) Boyd, G. D.; Buehler, E.; Storz, F. G. Linear and nonlinear optical properties of $ZnGeP_2$ and CdSe. *Appl. Phys. Lett.* **1971**, *18*, 301−304.
(7) Meng, J.; Liu, G.; Zhang, W.; Zhao, L.; Liu, H.; Jia, X.; Mu, D.; Liu, S.; Dong, X.; Zhang, J.; Lu, W.; Wang, G.; Zhou, Y.; Zhu, Y.; Wang, X.; Xu, Z.; Chen, C.; Zhou, X. J. Coexistence of Fermi arcs and Fermi pockets in a high-T_c copper oxide superconductor. *Nature* **2009**, *462*, 335−338.
(8) Zhou, Y.; Wang, G.-L.; Li, C.-M.; Peng, Q.-J.; Cui, D.-F.; Xu, Z.-Y.; Wang, X.-Y.; Zhu, Y.; Chen, C.-T.; Liu, G.-D.; Dong, X.-L.; Zhou, X.-J. Sixth harmonic of a Nd:YVO_4 laser generation in KBBF for ARPES. *Chin. Phys. Lett.* **2008**, *25*, 963−965.
(9) Sun, Z.; Yi, Y.; Song, T.; Clark, G.; Huang, B.; Shan, Y.; Wu, S.; Huang, D.; Gao, C.; Chen, Z.; McGuire, M.; Cao, T.; Xiao, D.; Liu, W.-T.; Yao, W.; Xu, X.; Wu, S. Giant nonreciprocal second-harmonic generation from antiferromagnetic bilayer CrI_3. *Nature* **2019**, *572*, 497−501.
(10) Fiebig, M.; Pavlov, V. V.; Pisarev, R. V. Second-harmonic generation as a tool for studying electronic and magnetic structures of crystals: review. *J. Opt. Soc. Am. B* **2005**, *22*, 96−118.
(11) Wuttig, M.; Yamada, N. Phase-change materials for rewriteable data storage. *Nat. Mater.* **2007**, *6*, 824−832.
(12) Wuttig, M. Phase-change materials: Towards a universal memory? *Nat. Mater.* **2005**, *4*, 265−266.
(13) Zhang, Y.; Zhang, W.; Li, S.-H.; Ye, Q.; Cai, H.-L.; Deng, F.; Xiong, R.-G.; Huang, S. D. Ferroelectricity induced by ordering of twisting motion in a molecular rotor. *J. Am. Chem. Soc.* **2012**, *134*, 11044−11049.
(14) Ye, H.-Y.; Tang, Y.-Y.; Li, P.-F.; Liao, W.-Q.; Gao, J.-X.; Hua, X.-N.; Cai, H.; Shi, P.-P.; You, Y.-M.; Xiong, R.-G. Metal-free three-dimensional perovskite ferroelectrics. *Science* **2018**, *361*, 151−155.
(15) Cai, H.; Zhang, W.; Ge, J.-Z.; Zhang, Y.; Awaga, K.; Nakamura, T.; Xiong, R.-G. 4-(cyanomethyl)anilinium perchlorate: A new displacive-type molecular ferroelectric. *Phys. Rev. Lett.* **2011**, *107*, 147601.
(16) Mao, H.-K.; Chen, X.-J.; Ding, Y.; Li, B.; Wang, L. Solids, liquids, and gases under high pressure. *Rev. Mod. Phys.* **2018**, *90*, No. 015007.
(17) Wisser, M. D.; Chea, M.; Lin, Y.; Wu, D. M.; Mao, W. L.; Salleo, A.; Dionne, J. A. Strain-induced modification of optical selection rules in lanthanide-based upconverting nanoparticles. *Nano Lett.* **2015**, *15*, 1891−1897.
(18) Bayarjargal, L.; Winkler, B. Second harmonic generation measurements at high pressures on powder samples. *Z. Kristallogr. - Cryst. Mater.* **2014**, *229*, 92−100.
(19) Pinnick, D. A.; Lee, S. A.; Sun, X.; Simon, H. J. Optical second-harmonic-generation study of quartz up to 31 GPa. *Phys. Rev. B: Condens. Matter Mater. Phys.* **1997**, *55*, 8031−8033.
(20) Ruiz-Fuertes, J.; Bernert, T.; Zimmer, D.; Schrodt, N.; Koch-Müller, M.; Winkler, B.; Bayarjargal, L.; Popescu, C.; MacLeod, S.; Glazyrin, K. Ambient-temperature high-pressure-induced ferroelectric phase transition in $CaMnTi_2O_6$. *Phys. Rev. B: Condens. Matter Mater. Phys.* **2017**, *96*, No. 094101.
(21) Bayarjargal, L.; Winkler, B. Pressure-induced magnetic phase transition in Cr_2O_3 determined by second harmonic generation measurements. *Appl. Phys. Lett.* **2013**, *102*, 182403.
(22) Halasyamani, P. S.; Poeppelmeier, K. R. Noncentrosymmetric oxides. *Chem. Mater.* **1998**, *10*, 2753−2769.
(23) Chen, C.; Wu, Y.; Li, R. The anionic group theory of the non-linear optical effect and its applications in the development of new high-quality NLO crystals in the borate series. *Int. Rev. Phys. Chem.* **1989**, *8*, 65−91.
(24) Chen, C.; Wu, Y.; Li, R. The development of new NLO crystals in the borate series. *J. Cryst. Growth* **1990**, *99*, 790−798.
(25) Zhao, S.; Jiang, X.; He, R.; Zhang, S.-Q.; Sun, Z.; Luo, J.; Lin, Z.; Hong, M. A combination of multiple chromophores enhances second-harmonic generation in a nonpolar noncentrosymmetric oxide: $CdTeMoO_6$. *J. Mater. Chem. C* **2013**, *1*, 2906−2912.
(26) Liang, A.; Rahman, S.; Rodriguez-Hernandez, P.; Muñoz, A.; Manjón, F. J.; Nenert, G.; Errandonea, D. High-Pressure Raman Study of $Fe(IO_3)_3$: Soft-Mode Behavior Driven by Coordination Changes of Iodine Atoms. *J. Phys. Chem. C* **2020**, *124*, 21329−21337.
(27) Liang, A.; Popescu, C.; Manjon, F. J.; Rodriguez-Hernandez, P.; Muñoz, A.; Hebboul, Z.; Errandonea, D. Structural and vibrational study of $Zn(IO_3)_2$ combining high-pressure experiments and density-functional theory. *Phys. Rev. B: Condens. Matter Mater. Phys.* **2021**, *103*, No. 054102.
(28) Bu, K.; Luo, H.; Guo, S.; Li, M.; Wang, D.; Dong, H.; Ding, Y.; Yang, W.; Lü, X. Pressure-Regulated Dynamic Stereochemical Role of Lone-Pair Electrons in Layered Bi_2O_2S. *J. Phys. Chem. Lett.* **2020**, *11*, 9702−9707.
(29) Mao, H. K.; Xu, J.; Bell, P. M. Calibration of the ruby pressure gauge to 800 kbar under quasihydrostatic conditions. *J. Geophys. Res.* **1986**, *91*, 4673−4676.
(30) Prescher, C.; Prakapenka, V. B. DIOPTAS: A Program for Reduction of Two-Dimensional X-Ray Diffraction Data and Data Exploration. *High Pressure Res.* **2015**, *35*, 223−230.
(31) Rodriguez-Carvajal, J. Recent advances in magnetic structure determination by neutron powder diffraction. *Phys. B* **1993**, *192*, 55−69.
(32) Kortüm, G.; Braun, W.; Herzog, G. Principles and Techniques of Diffuse-Reflectance Spectroscopy. *Angew. Chem., Int. Ed. Engl.* **1963**, *2*, 333−341.
(33) Kurtz, S. K.; Perry, T. T. A Powder Technique for the Evaluation of Nonlinear Optical Materials. *J. Appl. Phys.* **1968**, *39*, 3798−3813.
(34) Forzatti, P.; Tieghi, G. Solid State Reactions to $CdTeMoO_6$ and Its Structural Characterization. *J. Solid State Chem.* **1978**, *25*, 387−390.
(35) Forzatti, P.; Trifirò, F.; Villa, P. L. $CdTeMoO_6$, $CoTeMoO_6$, $MnTeMoO_6$, and $ZnTeMoO_6$: A New Class of Selective Catalysts for Allylic Oxidation of Butene and Propylene. *J. Catal.* **1978**, *55*, 52−57.
(36) Laligant, Y. X-Ray and TEM Studies of $CdTeMoO_6$ and $CoTeMoO_6$: A New Superstructure of Fluorite Type with Cation and Anion Deficiencies (■CoTeMo)($\square_2O_6$). *J. Solid State Chem.* **2001**, *160*, 401−408.
(37) Bayarjargal, L.; Winkler, B.; Haussühl, E.; Boehler, R. Influence of deviatoric stress on the pressure-induced structural phase transition of ZnO studied by optical second harmonic generation measurements. *Appl. Phys. Lett.* **2009**, *95*, No. 061907.
(38) Jaffe, A.; Lin, Y.; Mao, W. L.; Karunadasa, H. I. Pressure-Induced Metallization of the Halide Perovskite $(CH_3NH_3)PbI_3$. *J. Am. Chem. Soc.* **2017**, *139*, 4330−4333.
(39) Zhang, L.; Liu, C.; Lin, Y.; Wang, K.; Ke, F.; Liu, C.; Mao, W. L.; Zou, B. Tuning Optical and Electronic Properties in Low-Toxicity Organic-Inorganic Hybrid $(CH_3NH_3)_3Bi_2I_9$ under High Pressure. *J. Phys. Chem. Lett.* **2019**, *10*, 1676−1683.
(40) Jaffe, A.; Lin, Y.; Mao, W. L.; Karunadasa, H. I. Pressure-Induced Conductivity and Yellow-to-Black Piezochromism in a Layered Cu-Cl Hybrid Perovskite. *J. Am. Chem. Soc.* **2015**, *137*, 1673−1678.
(41) Li, C.; Tian, X.; Gao, Z.; Wu, Q.; Zhao, P.; Sun, Y.; Zhang, C.; Zhang, S.; Cui, D.; Tao, X. Controlled Growth of Layered Acentric $CdTeMoO_6$ Single Crystals with Linear and Nonlinear Optical Properties. *Cryst. Growth Des.* **2018**, *18*, 3376−3384.
(42) Chan, M. K. Y.; Ceder, G. Efficient Band Gap Prediction for Solids. *Phys. Rev. Lett.* **2010**, *105*, 196403.
(43) Murugan, R. Investigation on ionic conductivity and Raman spectra of γ-Bi_2MoO_6. *Phys. B* **2004**, *352*, 227−232.
(44) Kongmark, C.; Martis, V.; Rubbens, A.; Pirovano, C.; Löfberg, A.; Sankar, G.; Bordes-Richard, E.; Vannier, R.; Van Beek, W. Elucidating the genesis of Bi_2MoO_6 catalyst by combination of synchrotron radiation experiments and Raman scattering. *Chem. Commun.* **2009**, 4850−4852.

https://doi.org/10.1021/acs.chemmater.1c00362
Chem. Mater. 2021, 33, 2929−2936

(45) Blasse, G.; Hordijk, W. The Vibrational Spectrum of Ni_3TeO_6 and Mg_3TeO_6. *J. Solid State Chem.* **1972**, *5*, 395−397.
(46) Llanos, J.; Castillo, R.; Barrionuevo, D.; Espinoza, D.; Conejeros, S. The family of Ln_2TeO_6 compounds (Ln = Y, La, Sm and Gd): Characterization and synthesis by the Pechini sol-gel process. *J. Alloys Compd.* **2009**, *485*, 565−568.

https://doi.org/10.1021/acs.chemmater.1c00362
Chem. Mater. 2021, 33, 2929−2936